Escola de Primavera de Transição e Turbulência
Blumenau 2022

ABCM
13th Spring School on Transition and Turbulence
September 19th-23rd, 2022, Blumenau, SC, Brazil

EPTT-2022-0003
BUBBLES COALESCENCE MODELING AND PHASE INTERACTIONS IN A SQUARED BUBBLE COLUMN

Ana Paula Moreira de Freitas
Federal University of Uberlândia, Uberlândia - MG
anapaulamorfre@gmail.com

Jonathan Utzig
University of Blumenau, Blumenau - SC
jutzig@furb.br

João Marcelo Vedovotto
Federal University of Uberlândia, Uberlândia - MG
vedovotto@ufu.br

Abstract. *In the present work, the influence of bubble coalescence on the continuous phase in bubble columns is studied. The Euler-Lagrange approach is used to describe the two-phase flow equations of motion. To map the free surface between the gas and the liquid, the Volume of Fluid (VoF) method is used, as well as the bubbles collisions tracking in the liquid medium is realized by the DPM method, considering the four-way coupling. The algorithm to solve the coalescence proposed by Sommerfeld* et al. *(2003) was implemented and verified in the MFSim computational package. The results showed good agreement with experimental data, despite new improvements in the model can be made.*

Keywords: *Coalescence, Bubble Column, Biphasic Flows, Euler-Lagrange Approach*

1. INTRODUCTION

The study of multiphase flows is of great applicability in industry and academia. Some examples are: pneumatic transport of particles, recovery of crude oil, movement of pollutants in the atmosphere, fuel injection in engines and particulate flow in cyclones. Due to the interactions between the different phases, these flows become difficult to describe theoretically. Therefore, Computational Fluid Dynamics (CFD) is a useful tool in the observations of the complex physics associated with multiphase flow.

To establish a two-phase flow, only two phases are needed. When the two phases are formed by different fluids, both are called continuous media. On the other hand, when one of them is a continuous medium and the other is spread out in this medium in a dispersion, the flow is formed by a continuous and a dispersed phase. In this work, the two-phase flow adopted is known as bubbling flow and is formed by the presence of bubbles scattered in the liquid medium. The Euler-Lagrange approach was used to resolve the continuous phase formed by the liquid and the dispersed phase formed by the bubbles.

For the study of bubbling flows, the so-called bubble columns are commonly used. Such columns can have a cylindrical or rectangular shape, according to the desired application. The column is partially filled with liquid, in the two-phase case, or liquid with suspended solids, in the multiphase case, having a liquid free surface in contact with gas at the top. Gas injection takes place at the bottom of the column through distributor plates, which can have different flow rates or formats that control the size of the bubbles created. The bubbles flow over the liquid to the free surface, joining the gas contained above the free surface. A schematic of a rectangular bubble column can be seen in the 1 below.

Among the main applications of bubble columns are reactions in chemical, biochemical, petroleum and metallurgical industries. Different types of chemical reactions, oxidation, chlorination, alkylation, polymerization, esterification and hydrogenation can be implemented in bubble columns (Leonard *et al.*, 2015).

Several studies have been carried out in recent decades with the objective of verifying the flow behavior in bubble columns and its sensitivity to column parameters, such as column shape and dimensions, gas injection flow, bubble dimensions and types of distributor boards, to name a few. In this way, the CFD comes as a viable and low-cost tool in carrying out these studies. It is possible to simulate and predict numerous conditions involving bubble columns.

The regimes normally found in bubble columns are: homogeneous regime and heterogeneous regime. The homogeneous regime can be classified into two sub-classifications: the perfectly bubbly flow, which occurs when the bubbles are spherical with approximately the same diameter; and the imperfect bubbly flow characterized by an approximately equal bubble size distribution. The heterogeneous regime is observed when there is a larger bubble size distribution where small and large bubbles coexist. In this regime, breakage and coalescence phenomena control the flow that is normally not controlled by the primary bubble in the gas distributor (Kantarci *et al.*, 2005). Leonard *et al.* (2015) makes an extensive study on the parameters that guide the transition between the mentioned regimes.

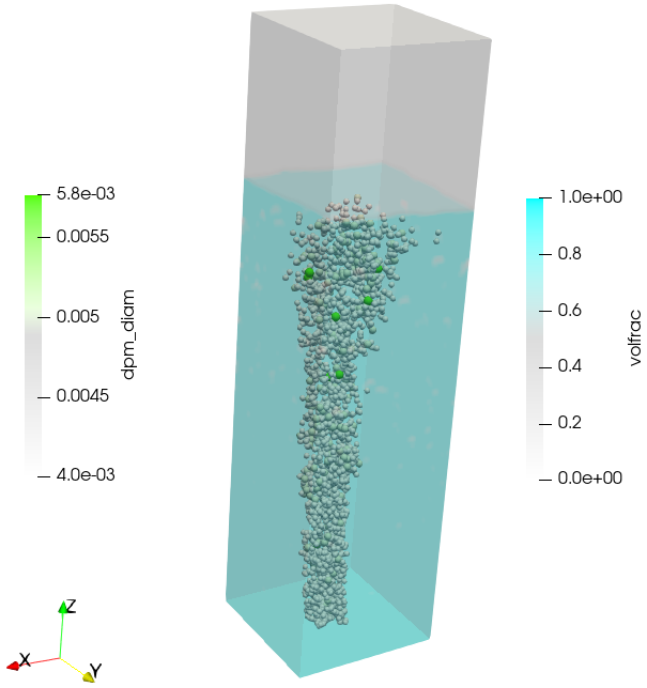

Figure 1. Illustration of a rectangular bubble column with bubble injection.

In the present work, the influence of bubble coalescence in a rectangular bubble column with dimensions $0.15 \times 0.15 \times 0.6\,[m]$ under specified conditions is investigated. The homogeneous regime was adopted and the model for coalescence proposed by Sommerfeld *et al.* (2003) was implemented in the MFSim computational package.

MFSim has been developed at MFLab/UFU in partnership with Petrobras and satisfactory results have been obtained using it to solve problems involving turbulent multiphase flows (Damasceno *et al.*, 2015; Barbi *et al.*, 2018), with phase change (Pinheiro and Vedovotto, 2019) and problems involving fluid-structure interactions (Neto *et al.*, 2019). One of the highlights of MFSim is the use of a structured block mesh with dynamic adaptive local refinement, allowing the refinement to occur in regions with greater formation of vortices, for example. In the case where simulations in Lagrangian referential are implemented in MFSim, the particulates (solid or liquid) are treated as elements of fluids (or solids) as particles. The tracking of these particles is based on the application of Newton's second law and proper models are needed for the collisions treatment. Thus, the implementation of a coalescence model comes to contribute to the development of the software and to evaluate the flow compared to experimental data. This work is organized as follows: first the models used to structure the bubble column simulation are described, then the algorithm implemented in MFSim is shown. Finally, the results are evaluated and the conclusions are presented.

2. MATHEMATICAL MODEL

The model consists of two coupled parts: the first one describes the motion of the liquid phase considering the gas-liquid free surface (VoF), while the second one describes the motion of the bubbles considering the collisions between themselves and the walls (DPM), in addition to the consideration of bubble coalescence (Prince and Blanch, 1990). The coupling is done as a source term in the liquid phase momentum balance equation considering the exchange of momentum between the gas and the liquid phase and vice versa (4-way coupling). Bubble dynamics and fluid-bubble coupling are described below.

2.1 Mass and momentum balance

The mass balance for the newtonian, incompressible and isothermal fluid phase is described by the continuity equation as:

$$\frac{\partial \epsilon_f}{\partial t} + \nabla \cdot (\epsilon_f \mathbf{u}_f) = 0 \tag{1}$$

where ϵ is the volumetric fraction and $\mathbf{u}$ is the velocity. The subscript f represents the fluid phase that contains the liquid (l) and gas (g) phases.

The momentum balance is described by the Navier-Stokes equation:

$$\rho_f \left[\frac{\partial (\epsilon_f \mathbf{u}_f)}{\partial t} + \nabla \cdot (\epsilon_f \mathbf{u}_f \mathbf{u}_f) \right] = -\epsilon_f \nabla p - \nabla \cdot (\epsilon_f \tau_f) + \rho_f \epsilon_f \mathbf{g} - \mathbf{f}_\sigma - \mathbf{f}_{l \to b} \tag{2}$$

where $\mathbf{f}_\sigma$ is the surface tension term and $\mathbf{f}_{l \to b}$ is the force term of the bubble-liquid interaction. The subscript b represents the bubbles. The equation 2 represents the momentum balance for multiphase flows, but if $\epsilon_f = 1$, we have the Navier-Stokes equation for single-phase flows.

2.2 Volume of Fluid Method

The Volume of Fluid (VOF) is an Eulerian method used to approximate free boundaries in a numerical simulation, following regions of fluid interface. A scalar function F is used within a control volume to determine the fractional amount of liquid in a cell in the computational mesh. Thus:

$$F = \frac{\epsilon_l}{\epsilon_f} \frac{\epsilon_l}{(\epsilon_l + \epsilon_g)}. \tag{3}$$

The motion of the fluid phase, formed by the liquid and the gas, is described by the transport equation:

$$\frac{DF}{Dt} = \frac{\partial F}{\partial t} + \mathbf{u}_f \cdot \nabla F = 0. \tag{4}$$

The density of the fluid phase is determined from the equation:

$$\rho_f = F\rho_l + (1 - F)\rho_g. \tag{5}$$

Finally, the expression to obtain the local average viscosity of the fluid is calculated from the harmonic average of the kinematic viscosity of the liquid and gas phases (Deepak *et al.*, 2014):

$$\frac{\rho_f}{\mu_f} = F\frac{\rho_l}{\mu_l} + (1 - F)\frac{\rho_g}{\mu_g}. \tag{6}$$

2.3 Bubbles tracking

The motion of each bubble in the flow is derived from Newton's Second Law. Considering incompressible bubbles:

$$\rho_b V_b \frac{d(\mathbf{v_b})}{dt} = \Sigma \mathbf{F_b}, \tag{7}$$

where ρ_b, V_b and $\mathbf{v_b}$ are the density, volume and velocity of the bubble, respectively. The sum of the forces $\mathbf{F_b}$ in the term on the right side of the equation represents the different forces acting on the bubbles. The forces considered in this work were: Weight and Thrust, Drag Force, Shear Lift Force and Virtual Mass. The equations are presented below, respectively:

$$F_{GP} = m_b g \left(1 - \frac{\rho_l}{\rho_g} \right) \tag{8}$$

where g is the acceleration due to gravity and m_b is the mass of the bubble.

For the drag force is used:

$$F_D = \frac{\rho_l}{2} \frac{\pi}{4} D_b v_{rel}^2 C_D \tag{9}$$

where v_{rel} is the relative velocity between the liquid and the bubble, D_b is the bubble diameter, and C_D is the drag coefficient calculated from the bubbles Reynolds number (Re_b)]:

$$C_D = \begin{cases} \frac{24}{Re_b}, & \text{for } 0 < Re_b \leq 0.1, \\ \frac{24}{Re_b}(1 + 0.15Re_b^{0.687}), & \text{for } 0.1 \leq Re_b \leq 1000, \\ 0.44 & \text{for } Re_b > 1000. \end{cases} \tag{10}$$

The Shear Lift Force is calculated through:

$$F_L = \frac{\rho_l}{2}\frac{\pi}{4}D_b^3 C_L[(\mathbf{u_l} - \mathbf{v_b}) \times \nabla \times \mathbf{u_l}] \tag{11}$$

where $\mathbf{u_l}$ and $\mathbf{v_b}$ are the liquid and bubble velocities, respectively. C_L is the lift coefficient calculated by (Saffman, 1965, 1968; Renwei and Klausner, 1987):

$$C_L = \begin{cases} \frac{4.1126}{\sqrt{Re_s}}[(1 - 0,3314\beta^{0.5})exp(-0.1Re_b) + 0.3314\beta^{0.5}], & \text{for } Re_b \leq 40, \\ \frac{4.1126}{\sqrt{Re_s}}[0.0524(\beta Re_b)^{0.5}], & \text{for } Re_b \leq 40, \end{cases} \tag{12}$$

where $\beta = 0.5\frac{Re_s}{Re_b}$ for $0.005 < \beta < 0.4$. And Re_s is the Reynolds number of the shear flow given by:

$$Re_s = \frac{\rho_l D_b^2 ||\nabla \times \mathbf{u_l}||}{\mu_l} \tag{13}$$

where μ_l is the viscosity of the liquid. Finally, the virtual mass force can be obtained from:

$$F_{VM} = \frac{\rho_l}{2}\frac{\pi}{6}D_b^3 C_{VM}\left(\frac{D\mathbf{u_l}}{Dt} - \frac{d\mathbf{v_b}}{dt}\right) \tag{14}$$

where $C_{VM} = 0.5$ is the added mass coefficient (Deepak *et al.*, 2014).

2.4 Bubbles Coalescence

Collisions are resolved deterministically using the rigid sphere model from Hoomans *et al.* (1996). After the collision, the bubbles interact for a while and some phenomena can occur. They are: *bouncing*, *reflexive separation*, *stretching separation*, *coalescence* and *shattering* .

In this work, the phenomenon of coalescence was considered to evaluate the bubble column flow. The bubble coalescence model proposed by Sommerfeld *et al.* (2003) is used to determine whether the collision will result in coalescence or not. The contact time is compared with the drainage time of the film formed by the contact of two bubbles, which is calculated by the Prince and Blanch (1990) model. If the film drainage time is less than the bubble contact time, it indicates film breakage and coalescence occurs. In this way, the bubble contact time and the film drainage time can be calculated, respectively:

$$t_{contact} = \frac{C_C R_{ij}}{|v_{rel,b}|}, \tag{15}$$

$$t_{drainage} = \sqrt{\frac{R_{ij}^3 \rho_l}{16\sigma}} \ln\frac{h_0}{h_f}, \tag{16}$$

where h_0 is the initial thickness of the film and h_f its final thickness just before breaking. These values depend on the considered system, so experiments are necessary to obtain better estimates (Sommerfeld *et al.*, 2003). $v_{rel,b}$ is the relative velocity between the two bubbles. The equivalent bubble radius for a system of two interacting bubbles of different sizes is obtained as the harmonic mean of the radii of these two bubbles, R_b (Chesters and Hofman, 1982):

$$R_{ij} = 2\left(\frac{1}{R_{b,i}} + \frac{1}{R_{b,j}}\right)^{-1}. \tag{17}$$

In Eq. 15, where C_C represents the ratio between the deformation distance and the effective radius of the bubble and can be considered as a calibration constant. It is then noted that the contact time is a stochastic value that explains the randomness of the bubble motion induced by the turbulence, and that it is expressed by the normal component of the relative velocity of the impact.

The properties of the new bubble in case of coalescence are obtained from the mass and momentum balances. The new bubble diameter and the number of actual bubbles are given by Sommerfeld *et al.* (2003), respectively:

$$D^*_{b,1} = \left(D^3_{b,1} + D^3_{b,2}\right)^{1/3}, \tag{18}$$

$$N^*_{b,1} = N_{b,1}\left(\frac{D_{b,1}}{D^*_{b,1}}\right)^3. \tag{19}$$

The velocity components of the new bubble in the coordinate system can be obtained as:

$$\mathbf{v}^*_{\mathbf{b,1}} = \left(\frac{m_{b,1}\mathbf{v_{b,1}} + m_{b,2}\mathbf{v_{b,2}}}{m_{b,1} + m_{b,2}}\right). \tag{20}$$

3. COMPUTATIONAL METHODOLOGY

The simulation of the gas-liquid flow in the presented bubble column uses the algorithm shown in Fig. 2, implemented in the MFSim computational package. The energy transfer between the phases is given by the forces calculation as the gas is injected at the column bottom and the bubbles rise through the liquid. At each Lagrangian time step, the collision probability is computed from the bubbles trajectories. When a collision is identified, the algorithm is called, the contact and drainage time are calculated, the coalescence occurrence is determined and the new bubble properties are updated. One of the colliding Lagrangian entities is kept as the new bubble born, while the other one is deleted from the computation.

The simulation parameters, operating conditions, fluid properties and column dimensions are shown in the Tab. 1 below. The flow was simulated for a period of $150\,s$. The data was averaged over the last $120\,s$ and the results are analyzed in the next section.

Table 1. Operating conditions, column dimensions, fluids properties and numerical parameters used in the present study.

Parameter	**Value**
Liquid Density	$1000\,[kg/m^3]$
Gas Density	$1.2\,[kg/m^3]$
Liquid Viscosity	$1.0 \times 10^{-3}\,[Pa \cdot s]$
Gas Viscosity	$1.802 \times 10^{-5}\,[Pa \cdot s]$
Surface Tension	$0.073\,[N/m]$
Coalescence factor, C_C	0.1
Initial film thickness, h_0	$1.0\,[mm]$
Final film thickness, h_f	$0.1\,[mm]$
Column Dimension $(W \times D \times H)$	$0.15 \times 0.15 \times 0.6\,[m]$
Initial liquid height	$0.45\,[m]$
Initial Bubble diameter	$4.0 \times 10^{-3}\,[m]$
Number of bubbles to be injected at each step	1000
Number of grid cells $(NX \times NY \times NZ)$	$64 \times 64 \times 256$
Simulation time	$150\,[s]$

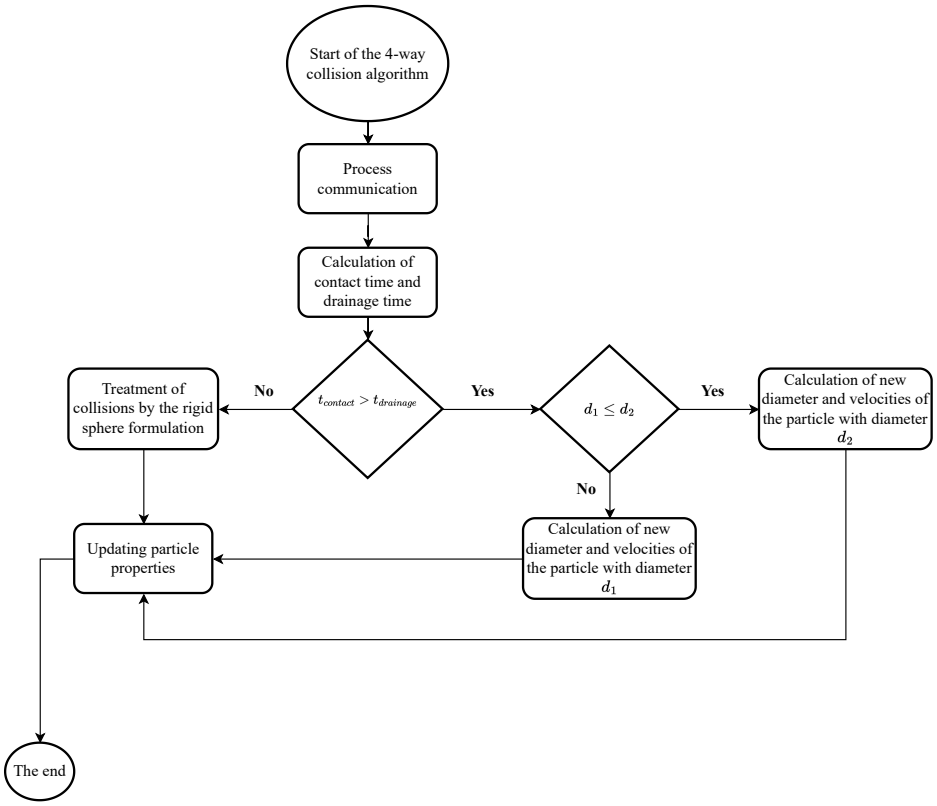

Figure 2. The bubbles coalescence algorithm implemented in the MFSim code.

4. RESULTS AND DISCUSSIONS

The gas-liquid flow in a bubble column was described. In this section, the simulation results are discussed. Liquid transversal mean and fluctuating velocity profiles are calculated at $z = 0.25\,m$ (as the Fig. 1 coordinates), in order do compare with the experimental data presented by Deen *et al.* (2000). It was added kitchen salt into the liquid used in the experiments by the authors to avoid bubbles coalescence and made the Particle Image Velocimetry (PIV) clearer. Indeed, the mathematical model proposed in the present work was solved with and without the bubbles coalescence, as well as considering the two- and four-way coupling with the liquid phase.

These model variations were done looking for better understanding of the computational code and the physics behind the bubble column phenomena. The Lagrangian and collision modeling should be verified and validated to light entities as gas bubbles. The first relevant comparison is between both four-way coupling results, i.e. the coalescing and non-coalescing effects on the liquid phase. It is worth mentioning that the experimental data validations makes sense only with the four-way non-coalescing results, given the liquid mixture cited above.

The liquid movement induced by the rising bubbles can be analyzed from its velocity components. In the Fig. 3, the transversal component of the mean fluctuating velocity is shown. The central region of the column presents the higher fluctuations because of the presence of the plume. Instead of symmetrical behavior as expected to a mean flow, both numerical and experimental data present some asymmetry due to non-stationary statistics. Besides that, there is a remarkable validation to all tested modelings, i.e. the bubbles collision and coalescence have negligible effect on this variable.

On the other hand, if all fluctuating components are assessed throughout the liquid kinetic energy, differences are observed between the modelings, as presents the Fig. 4. Bimodal profiles result from the non-coalescing simulations, likewise the experimental measurements. Two peaks and a central region with lower energy are caused by the bubble plume boundary, which dissipates the energy through the walls, were the velocity is zero and the experimental data cannot be acquired. The two-way solution, when the bubble collisions are not accounted for, presents the higher amount of energy since it is not transferred and dissipated between the bubbles. In this way, the case with bubbles coalescence presents lower energy transferred to the liquid phase due to collisions and coalescence occurred in the gas phase that consumed energy. It is also shown in Fig. 4 a gap between the experimental data and the simulations. This contrast is given by the period of time that both results were taken: the experimental one, Deen *et al.* (2000) acquired the PIV shots over $900\,s$ along the stable flow condition, while the simulation results were averaged for $120\,s$ starting at $30\,s$, along the transitional condition, as shown in Fig. 5 which illustrates the axial velocity of the liquid over time.

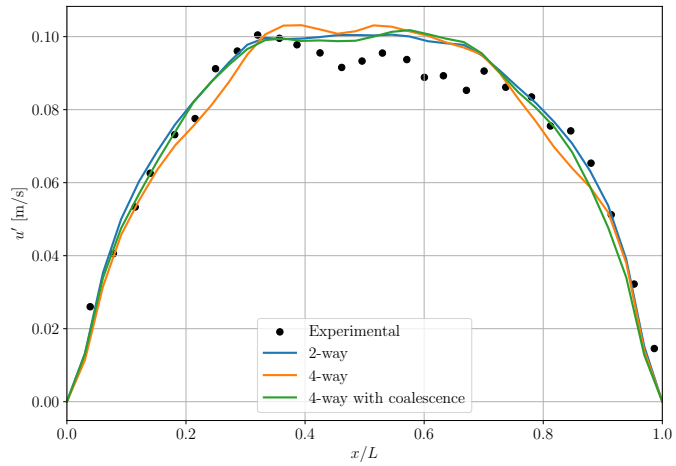

Figure 3. Mean transversal fluctuating liquid velocity, $z = 0.25\,[m]$: experimental data, two- and four-way coupling without coalescence, and four-way coupling with coalescence model.

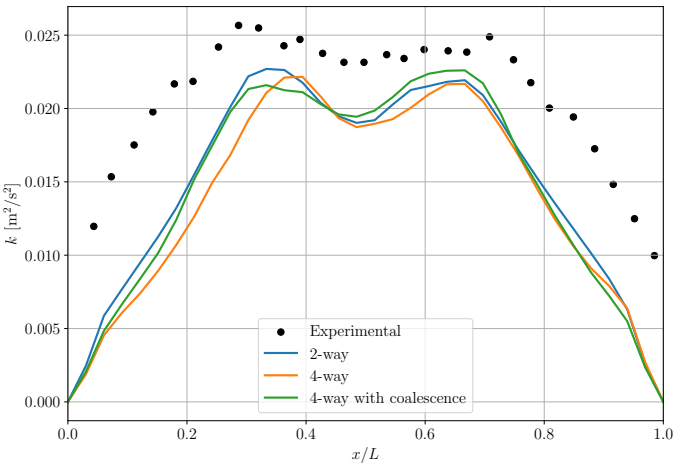

Figure 4. Mean liquid kinetic energy, $z = 0.25\,[m]$: experimental data, two- and four-way coupling without coalescence, and four-way coupling with coalescence model.

The axial mean and fluctuating velocities show even larger difference between the experimental data and the simulations, as present Fig. 6 and Fig. 7. The reason is the same as stated above to the liquid kinetic energy. However, there is an overprediction by twice the mean axial liquid velocity at the column center. As the bubble plume is rising mainly concentrated in the central region along the transitional period, it does not started to oscillate crosswise as the "snake effect", the global energy is kept in the vertical component. For the same reason the velocity fluctuation is lower in this direction at this time. No significant difference is seen in the mean axial velocity profiles, while the coalescing case caused lower fluctuation on the liquid phase. As the simulations run more time, the plume should start to oscillate crosswise, it will spread out the energy transfer and stimulate more bubble collisions and coalescence, which will result in a more prominent difference between the cases.

5. CONCLUSIONS

The implementation of the coalescence model proposed by Sommerfeld *et al.* (2003) was done in the in-house MFSim code. Euler-Lagrange simulations were performed and the non-coalescence model was validated according to data found in the literature Deen *et al.* (2000). The dynamics of the free surface at the gas-liquid interface was observed in the simulations. The coalescence model was studied and it was noted that for a coalescence factor of 0.1, the phenomenon is dominant at the beginning of the simulation.

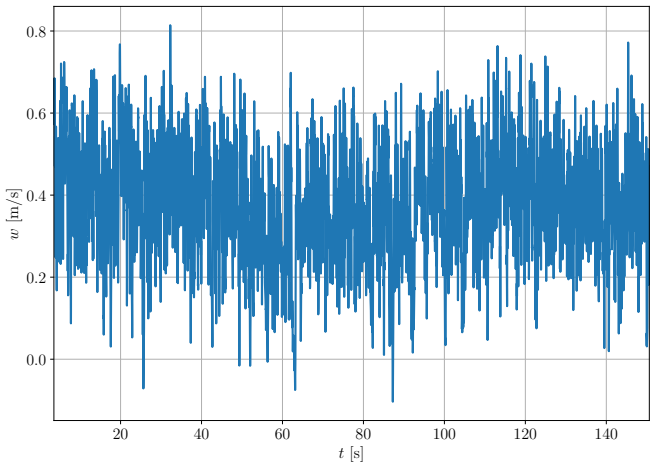

Figure 5. Temporal history of the axial velocity of the liquid at the center of the column, at the height of $z = 0.25\,[m]$.

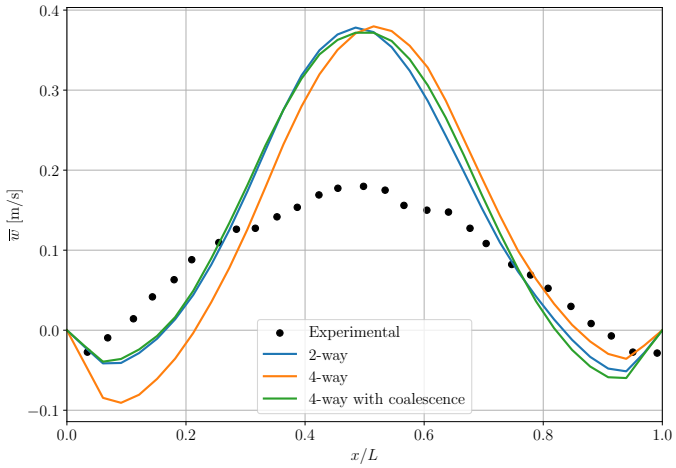

Figure 6. Mean axial liquid velocity, $z = 0.25\,[m]$: experimental data, two- and four-way coupling without coalescence, and four-way coupling with coalescence model.

6. ACKNOWLEDGEMENTS

The authors would like to thank Foz do Chapecó, Baesa, Enercan and Ceran for technical and financial support, through the Research and Development project PD-02949-3007/2022 – "Solução integrada para o diagnóstico de defeitos, análise dinâmica e monitoramento contínuo de unidades geradoras francis" with resources from ANEEL's RD program. The authors also would like to thank Petrobras, CNPq, FAPEMIG, and CAPES (INCT-EIE) for the financial support of the present contribution.

7. REFERENCES

Barbi, F., Pivello, M.R., Villar, M.M., Serfaty, R., Roma, A.M. and Silveira-Neto, A., 2018. "Numerical experiments of ascending bubbles for fluid dynamic force calculations". *Journal of the Brazilian Society of Mechanical Sciences and Engineering*.

Chesters, A.K. and Hofman, G., 1982. "Bubble coalescence in pure liquids". *Applied Scientific Research*.

Damasceno, M.M.R., Vedovotto, J.M. and Silveira-Neto, A., 2015. "Turbulent inlet conditions modeling using large-eddy simulations". *Computer Modeling in Engineering and Sciences*.

Deen, N.G., Hjertager, B.H. and Solberg, T., 2000. "Comparison of piv and lda measurement methods applied to the gas-liquid flow in a bubble column". *10th Int. Symp. on Appl. of Laser Techniques to Fluid Mech.*

Deepak, J., Kuipers, J.A.M. and Deen, N.G., 2014. "Numerical study of coalescence and breakup in a bubble column

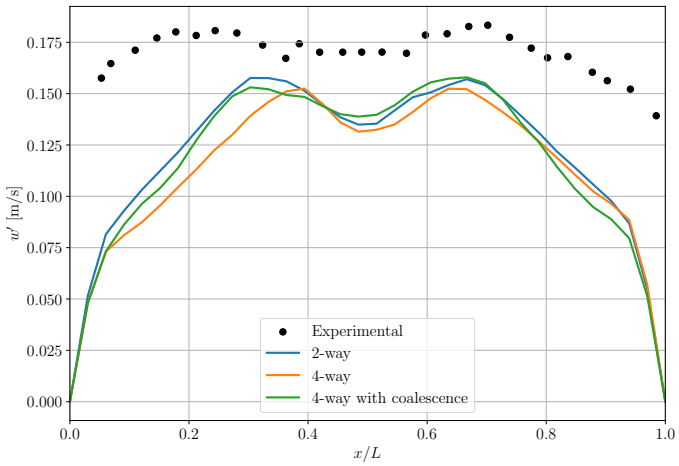

Figure 7. Mean axial fluctuating liquid velocity, $z = 0.25\,[m]$: experimental data, two- and four-way coupling without coalescence, and four-way coupling with coalescence model.

using a hybrid volume of fluid and discrete bubble model approach". *Chemical Engineering Science*, Vol. 119, pp. 134–146.

Hoomans, B.P.M., Kuipers, J.A.M., Briels, W.J. and Swaaij, W.P.M.V., 1996. "Discrete particle simulation of bubble and slug formation in a two-dimensional gas-fluidised bed: a hard-sphere approach".

Kantarci, N., Borak, F. and Ulgen, K.O., 2005. "Bubble column reactors". *Process Biochemistry*, Vol. 40, pp. 2263–2283.

Leonard, C., Ferrasse, J.H., Boutin, O., Lefevre, S. and Viand, A., 2015. "Bubble column reactors for high pressures and high temperatures operation". *Chemical engineering research and design*, Vol. 100, p. 391–421.

Neto, H.R., Cavalini, A., Vedovotto, J.M. and Silveira-Neto, A., 2019. "Influence of seabed proximity on the vibration responses of a pipeline accounting for fluid-structure interaction". *Mechanical Systems and Signal Processing*.

Pinheiro, A.P. and Vedovotto, J.M., 2019. "Evaluation of droplet evaporation models and the incorporation of natural convection effects". *Flow, Turbulence and Combustion*.

Prince, M.J. and Blanch, H.W., 1990. "Bubble coalescence and break-up in airsparged bubble columns". *AIChE Journal*, Vol. 36, pp. 1485–1499.

Renwei, M. and Klausner, J.F., 1987. "Shear lift force on spherical bubbles". *J. Fluid Mech*, Vol. 183, pp. 190–218.

Saffman, P.G., 1965. "The lift on a small sphere in a slow shear flow". *J. Fluid Mech*, Vol. 22, pp. 385–400.

Saffman, P.G., 1968. "Corrigendum to "the lift on a small sphere in a slow shear flow"". *J. Fluid Mech*, Vol. 31, p. 624.

Sommerfeld, M., Bourloutski, E. and Bröder, D., 2003. "Euler/lagrange calculations of bubbly flows with consideration of bubble coalescence". Vol. 81, pp. 508–518.

8. RESPONSIBILITY NOTICE

The authors are the only responsible for the printed material included in this paper.